# Overtones of isoscalar giant resonances in medium-heavy and heavy nuclei

M. L. Gorelik,[1] I. V. Safonov,[1] and M. H. Urin[1,2]

[1]*Moscow Engineering Physics Institute (State University), 115409 Moscow, Russia*
[2]*Kernfysisch Versneller Institute, 9747 AA Groningen, The Netherlands*

A semimicroscopic approach based on both the continuum random-phase-approximation method and a phenomenological treatment of the spreading effect is extended and applied to describe the main properties (particle-hole strength distribution, energy-dependent transition density, partial direct-nucleon-decay branching ratios) of the isoscalar giant dipole, second monopole, and second quadrupole resonances. The abilities of the approach are checked by description of the gross properties of the main-tone resonances. Calculation results obtained for the resonances in a few singly- and doubly-closed-shell nuclei are compared with available experimental data.

## I. INTRODUCTION

Experimental and theoretical studies of high-energy giant resonances (GRs) have been undertaken in recent years to understand better how the different characteristics associated with GR formation (concentration of the particle-hole strength, coupling to the continuum, the spreading effect) are affected with increasing the GR energy. Many of the known high-energy GRs are the next vibration modes (the overtones) relative to the corresponding low-energy GRs (the main tones). The lowest-energy overtone is the isoscalar giant dipole resonance (ISGDR) experimentally studied in a few medium-heavy and heavy nuclei via the $(\alpha, \alpha')$ reaction [1–4]. The ISGDR is the overtone of the $1^-$ zero-energy spurious state (SS), associated with center-of-mass motion. The experimental results of Refs. [1–4] are concerned with distribution of the corresponding dipole strengths. Only recently have the direct nucleon decays of the ISGDR been observed, using the $(\alpha, \alpha'N)$ reactions [5–7]. These studies are planned to be continued [8]. The isovector giant charge exchange (in the $\beta^-$ channel) monopole and spin-monopole resonances are the overtones of the isobaric analogue and Gamow-Teller resonances, respectively. These overtones have been studied via charge-exchange reactions [9,10]. Direct proton decays of the giant spin-monopole resonance have been recently observed using the $(^3\text{He}, tp)$ reaction [10]. Other candidates for studies of high-energy GRs are the overtones of the isoscalar giant monopole and quadrupole resonances (ISGMR2 and ISGQR2, respectively). The corresponding main tones, having relatively low energy, have been experimentally studied at some length [1–3]. However, evidence for the existence of the ISGQR2 has been reported for the first time only recently [5,6].

Theoretical studies of the isoscalar overtones deal primarily with the ISGDR. Microscopically, this GR is mainly due to $3\hbar\omega$ particle-hole-type excitations, while the overtones of the isoscalar quadrupole and monopole GRs are mainly due to $4\hbar\omega$ excitations. The first microscopic calculations of the strength distribution for the ISGDR and for all the above-mentioned isoscalar overtones were done in the 1980s (Refs. [11,12], respectively). In recent years Hartree-Fock +random phase approximation (RPA) calculations with the use of the Skyrme interactions have been done to specify the ISGDR energy and, after comparing with experimental data, to draw conclusions about the nuclear incompressibility [13,14]. Similar goals are pursued in the approaches based on the relativistic version of the RPA and on the semiclassical treatment of nuclear vibrations (see, e.g., Refs. [15,16], respectively). However, the microscopic structure and "differential" properties of high-energy GRs, which correspond to collective excitations of nuclei as finite-size open Fermi systems, are of particular interest. Attempts to describe the main properties (the strength distribution, energy-dependent transition density, partial direct-nucleon-decay branching ratios) of the ISGDR have been undertaken in Refs. [17,18] within a semimicroscopic approach, based on both the continuum RPA (CRPA) method and a phenomenological treatment of the spreading effect. In these references the gross properties (parameters of the strength distribution, transition density) have been satisfactorily described for the ISGDR in a few medium-heavy and heavy nuclei. Unlike the gross properties, the partial branching ratios for direct nucleon decay of a particular GR carry information about its microscopic structure and also about its coupling to the continuum and the spreading effect. Initial attempts (undertaken in Refs. [17,18] for the ISGDR in $^{208}$Pb) to calculate the partial direct-nucleon-decay branching ratios ran into difficulties associated with taking the spreading effect into account. A way to overcome these difficulties was given in Ref. [19]. The overtone of the isoscalar monopole resonance was theoretically studied within a CRPA-based approach in Ref. [20] mainly to search for narrow ("trapped") resonances, having a small relative strength. The gross properties of the ISGMR2 are described in Ref. [21], where both the microscopic Hartree-Fock+RPA approach with the use of the Skyrme interactions and a semiclassical approach have been employed. Within the semimicroscopic approach, the main properties of this resonance are briefly described in Ref. [19].

Motivated by aspirations to describe both the main properties of high-energy GRs and forthcoming experimental data concerned with the isoscalar overtones, we pursue the following goals in the present work.

**69** 054322-1

TABLE I. The peak energy, total width (both in MeV), and parameters $\eta_L$ (in fm$^2$) calculated for the $L=0,1,2$ isoscalar GRs in the nuclei under consideration. The corresponding experimental values (given with errors) are taken from Ref. [3] ($L=0,1$) and Ref. [28] ($L=2$).

| | $^{58}$Ni | $^{90}$Zr | $^{116}$Sn | $^{144}$Sm | $^{208}$Pb |
|---|---|---|---|---|---|
| | | | ISGMR | | |
| $\omega_{peak}$ | 17.7 | 16.2 | 15.7 | 14.8 | 13.6 |
| | | 16.6±0.1 | 15.4±0.1 | 15.3±0.1 | 13.4±0.2 |
| $\Gamma$ | 4.4 | 4.2 | 4.0 | 3.9 | 3.9 |
| | | 4.9±0.2 | 5.5±0.3 | $3.7^{+0.1}_{-0.6}$ | 4.0±0.4 |
| | | | ISGQR | | |
| $\omega_{peak}$ | 14.7 | 12.7 | 11.9 | 11.2 | 10.0 |
| | | 14.0±0.2 | 13.2±0.2 | 12.2±0.2 | 11.0±0.2 |
| $\Gamma$ | 2.8 | 2.65 | 2.6 | 2.4 | 2.2 |
| | | 3.4±0.2 | 3.3±0.2 | 2.4±0.2 | 2.7±0.3 |
| | | | ISGDR | | |
| $\eta_{L=1}$ | 22.71 | 29.28 | 34.74 | 39.74 | 51.07 |
| $\omega^{LE}_{peak}$ | 9.21[a] | 12.1 | 9.3 | 12.0 | 7.02[b] |
| | | 17.8±0.5 | 15.6±0.5 | 14.2±0.2 | 13.0±0.1 |
| $\omega^{HE}_{peak}$ | 27.4 | 26.0 | 26.1 | 25.0 | 22.9 |
| | | 26.9±0.7 | 25.4±0.5 | $25.0^{+1.7}_{-0.3}$ | 22.7±0.2 |
| | | | ISGMR2 | | |
| $\eta_{L=0}$ | 42.04 | 52.75 | 55.57 | 54.50 | 75.25 |
| $\omega^{HE}_{peak}$ | 30.8 | 29.9 | 32.0 | 33.8 | 32.1 |
| | | | ISGQR2 | | |
| $\eta_{L=2}$ | 24.38 | 30.50 | 35.90 | 40.41 | 52.54 |
| $\omega^{HE}_{peak}$ | 32.9 | 34.6 | 34.1 | 32.8 | 30.5 |

[a]The LE component has an additional maximum at 12.1 MeV.
[b]The LE component has an additional maximum at 11.4 MeV.

(i) Extension of the CRPA-based semimicroscopic approach to describe direct nucleon decay of high-energy GRs;

(ii) description of the gross properties of the isoscalar main-tone resonances to check the abilities of the approach and to find the probing operators appropriate for overtone studies;

(iii) calculation of the partial direct-nucleon-decay branching ratios for the high-energy component of the IS-GDR;

(iv) description of the main properties of the second isoscalar giant monopole and quadrupole resonances; and

(v) comparison of the calculation results obtained for singly- and doubly-closed-shell nuclei $^{58}$Ni, $^{90}$Zr, $^{116}$Sn, $^{144}$Sm, and $^{208}$Pb, with available experimental data.

The paper is organized as follows. In Sec. II the basic elements, ingredients, and new points of the approach are presented. Section III contains calculation results and available experimental data on properties of the isoscalar giant main-tone and overtone resonances. A discussion of the results and concluding remarks are given in Sec. IV.

## II. BASIC ELEMENTS AND INGREDIENTS OF THE APPROACH

The continuum RPA method and a phenomenological treatment of the spreading effect are the basic elements of the semimicroscopic approach. In implementations of the approach the following phenomenological input quantities are used: a realistic nuclear mean field and the Landau-Migdal particle-hole interaction bound together by self-consistency conditions; an energy- and radial-dependent smearing parameter.

### A. CRPA equations

The CRPA equations are taken in the form accepted within Migdal's finite Fermi system theory [22]. As applied to description of isoscalar particle-hole-type excitations in closed-shell nuclei, these equations are given in detail in Refs. [17,18] and not shown here. [For the reader's convenience we use (in the main) the notation of Refs. [17,18] and sometimes refer to equations, tables, and figures from these references.] The nuclear polarizibility $P_L(\omega)$, strength function $S_L(\omega)$, and energy-dependent transition density $\rho_L(\vec{r},\omega)=\rho_L(r,\omega)Y_{LM}(\vec{n})$ ($\omega$ is the excitation energy) corresponding to an isoscalar probing operator $V_L(\vec{r})=V_L(r)Y_{LM}(\vec{n})$ can be calculated to describe gross properties of the corresponding isoscalar GR within the CRPA. The above-listed quantities are expressed via the radial part of the effective probing operators $\tilde{V}^\alpha_L(r,\omega)$ ($\alpha=n,p$ is the isotopic index), which are different from $V_L(r)$ due to core-
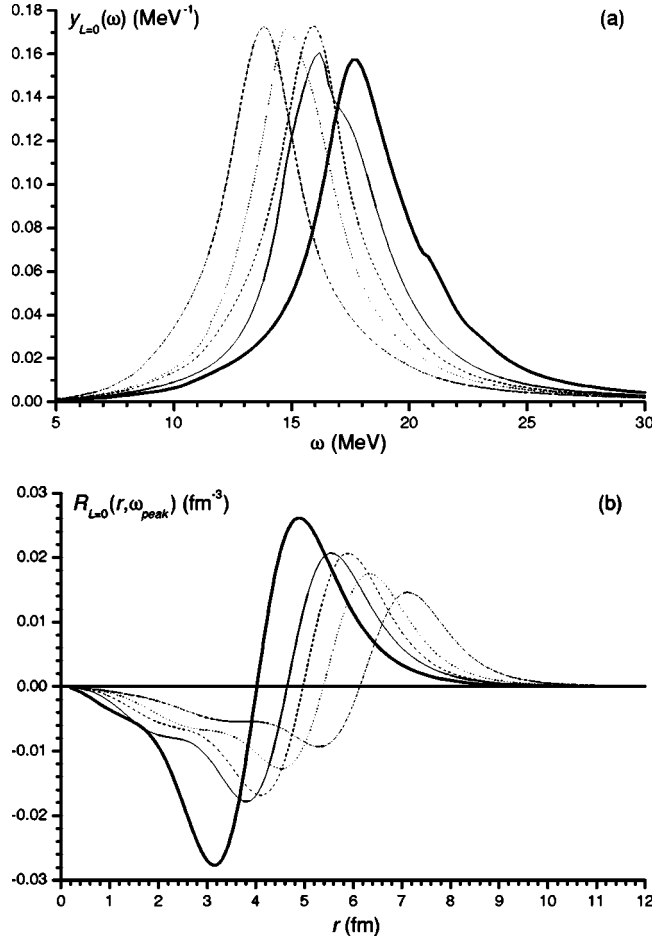
FIG. 1. (a) The relative energy-weighted strength function calculated for the ISGMR. (b) The reduced energy-dependent transition density calculated at the peak energy of the ISGMR (Table I). The thick, thin, dashed, dotted, and dash-dotted lines are for $^{58}$Ni, $^{90}$Zr, $^{116}$Sn, $^{144}$Sm, and $^{208}$Pb, respectively.
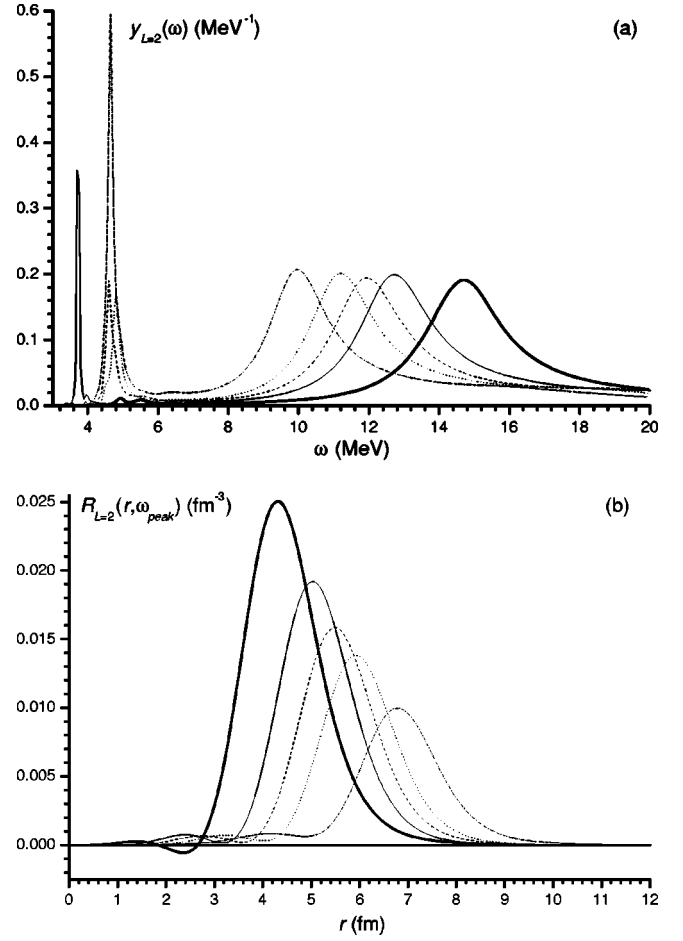


FIG. 2. (a) The relative energy-weighted strength function calculated for the ISGQR. (b) The reduced energy-dependent transition density calculated at the peak energy of the ISGQR (Table I). The notations on each graph are the same as in Fig 1.

polarization effects caused by the particle-hole interaction. The $\omega$ dependence of the above quantities comes from that of the free particle-hole propagator. The latter can be expressed in terms of occupation numbers $n_\mu^\alpha$, radial bound-state single-particle wave functions $\chi_\mu^\alpha$, and radial Green's functions $g_{(\lambda)}^\alpha(r,r',\epsilon_\mu\pm\omega)$ to take exactly the single-particle continuum into account [see Eqs. (1)–(3) of Ref. [17] and Eq. (1) of Ref. [18]].

When compared with Ref. [22], a new element of the CRPA equations is used within the approach-the direct-nucleon-escape amplitude $M_c^L(\omega)$ [see Eqs. (4),(5) of Ref. [17]]. This amplitude is proportional to the product of $(n_\mu^\alpha)^{1/2}$ and the matrix element of the corresponding radial effective operator taken with the use of the radial bound-state wave function $\chi_\mu^\alpha$ and the radial continuum-state wave function $\chi_{\epsilon,(\lambda)}^{(+)\alpha}$ [$\mu$ is the set of quantum numbers for an occupied single-particle level; $\epsilon=\epsilon_\mu+\omega$ and $(\lambda)$ are the energy and quantum numbers of an escaped nucleon, respectively, $c=\mu,(\lambda),\alpha$ is the set of nucleon-decay-channel quantum numbers compatible with the corresponding selection rules]. The $\omega$ dependence of the direct-nucleon-escape amplitude

comes not only from the effective probing operator, but also from the continuum-state wave function.

The partial direct-nucleon-decay branching ratio $b_c^L(\delta)$ can be reasonably defined as the ratio of the squared nucleon-escape amplitude integrated over a certain excitation-energy interval $\delta=\omega_1-\omega_2$ to the corresponding strength function integrated over the same interval. The total branching ratio $b_{\text{tot}}^L=\Sigma_c b_c^L$ is equal to unity for arbitrary interval $\delta$, as follows from the unitary condition, which is valid within the CRPA [Eq. (4) of Ref. [17]].

For comparison with the experimental branching ratios we sometimes replace the occupation numbers $n_\mu$ in the expression for $b_\mu^L=\Sigma_{(\lambda)}b_c^L$ with the corresponding experimental spectroscopic factors $S_\mu$. In this way, the coupling of single-hole states $\mu^{-1}$ populated after direct nucleon decay of GRs to low-energy collective states is taken into account phenomenologically.

In description of the gross properties of high-energy GRs, nucleon pairing in open-shell subsystems can be neglected with a high accuracy. To take into account the effect of nucleon pairing on the direct-nucleon-decay branching ratios in the CRPA equations, we replace the occupation numbers $n_\mu$ with the corresponding Bogoliubov factors $v_\mu^2$. The latter

TABLE II. Parameters of the ISGMR and ISGQR calculated for a certain excitation-energy interval. All the parameters are given in MeV except for $x$, which is given in percent.

| Nucleus | ISGMR | | | | ISGQR | | | |
|---|---|---|---|---|---|---|---|---|
| | $\omega_1 - \omega_2$ | $\bar{\omega}$ | $\Delta$ | $x$ | $\omega_1 - \omega_2$ | $\bar{\omega}$ | $\Delta$ | $x$ |
| $^{58}$Ni | 12–31 | 18.21 | 3.06 | 89 | 10–20 | 14.89 | 1.90 | 70 |
| $^{90}$Zr | 10–25 | 16.47 | 2.64 | 87 | 9–18 | 13.07 | 1.78 | 70 |
| $^{116}$Sn | 10–20 | 15.38 | 2.13 | 79 | 8–19 | 12.51 | 2.13 | 72 |
| $^{114}$Sm | 10–20 | 14.85 | 2.05 | 80 | 7–19 | 11.91 | 2.31 | 74 |
| $^{208}$Pb | 10–20 | 13.89 | 2.05 | 79 | 6–17 | 10.51 | 2.18 | 71 |

can be calculated in an isospin-self-consistent way with the use of experimental pairing energies [23]. To phenomenologically account for the coupling of single-quasiparticle states populated after direct nucleon decay to low-energy collective states, the calculated $b_\mu$ value is divided by $v_\mu^2$ and multiplied by $S_\mu$ [23].

An important aspect of the theoretical studies of GR overtones within the RPA is the choice of an appropriate probing operator. It is convenient to choose this operator with the condition that the main tone is not being excited. In this case the overtone exhausts most of the respective particle-hole strength. As applied to description of the ISGDR, charge-exchange giant monopole, and spin-monopole resonances, the choice of appropriate probing operators is discussed in Refs. [17,23,26], respectively. In particular, the radial part of the isoscalar second-order dipole probing operator $V_{L=1}^{(2)}(r) = r^3 - \eta_{L=1}r$ is used for description of the ISGDR. The parameter $\eta_{L=1}$ is defined by the condition: $\int \rho_{L=1}^{SS}(r)V_{L=1}^{(2)}(r)r^2dr = 0$, where $\rho_{L=1}^{SS}(r)$ is the spurious-state transition density. To describe the properties of the second isoscalar giant monopole and quadrupole resonances the radial part of the corresponding second-order probing operators is taken in the form $V_L^{(2)}(r) = r^4 - \eta_L r^2$. The parameters $\eta_L$ in this expression are determined by the condition

$$\int \rho_L(r, \omega_{peak})V_L^{(2)}(r)r^2dr = 0, \qquad (1)$$

where $\rho_L(r, \omega_{peak})$ is the radial part of the energy-dependent main-tone transition density taken at the peak energy of the main-tone strength function.

### B. Smearing procedure

Within the approach, the coupling of doorway states of the particle-hole type to many-quasiparticle configurations (i.e., the spreading effect) is taken into account phenomenologically in terms of an appropriate smearing parameter. Somewhat different smearing procedures are used for the description of low- and high-energy GRs. The aforementioned $\omega$-dependent quantities, calculated within the CRPA, for a low-energy ("sub-barrier") GR can be expanded in terms of nonoverlapping doorway-state resonances (of Breit-Wigner type) that have total escape widths $\Gamma^\uparrow$. To take into account the spreading effect in evaluating these energy-averaged $\omega$-dependent quantities, each doorway-state resonance is smeared independently. The smearing procedure lies in the replacement of $\Gamma^\uparrow$ by $\Gamma^\uparrow + I$, or equivalently, the replacement of $\omega$ by $\omega + iI/2$. The parameter $I$ (the mean doorway-state spreading width) is fitted to reproduce the experimental total width of the specific GR in calculations of the energy-averaged strength function. To calculate the energy-averaged direct-nucleon-escape amplitudes, it is also necessary to average the potential-barrier penetrability in a proper way, because the direct-escape nucleons have relatively low ("sub-barrier") energies. Thus, the energy-averaged transition density and the partial direct-nucleon-decay branching ratios can be evaluated within this approach without the use of any free parameters. This method has been employed in Ref. [17] to quantitatively describe the direct nucleon decay of ISGMR in a few nuclei. When applied to direct nucleon decay of the ISGDR in $^{208}$Pb, the method results only in qualitative description, however, because the corresponding doorway-state resonances have significant

TABLE III. Comparison of calculated and experimental parameters of the ISGMR and ISGDR. The experimental data (given with errors) are taken from Refs. [29,2], respectively. All the parameters are given in MeV.

| | | $^{90}$Zr | | $^{16}$Sn | | $^{208}$Pb | |
|---|---|---|---|---|---|---|---|
| ISGMR | $\bar{\omega}$ | 17.89±0.20 | 16.5 | 16.07±0.12 | 15.4 | 14.17±0.28 | 13.9 |
| | $\Delta$ | 3.14±0.09 | 2.6 | 2.16±0.08 | 2.1 | 1.93±0.15 | 2.1 |
| LE-ISGDR | $\bar{\omega}$ | 16.2±0.8 | 13.8 | 14.7±0.5 | 13.9 | 12.2±0.6 | 11.2 |
| | $\Delta$ | 1.9±0.7 | 2.1 | 1.6±0.5 | 2.0 | 1.9±0.5 | 1.9 |
| HE-ISGDR | $\bar{\omega}$ | 25.7±0.7 | 25.4 | 23.0±0.6 | 25.1 | 19.9±0.8 | 20.7 |
| | $\Delta$ | 3.5±0.6 | 3.5 | 3.7±0.5 | 3.2 | 2.5±0.6 | 2.4 |

TABLE IV. Comparison of calculated and experimental parameters of the ISGMR and ISGQR in $^{58}$Ni. The experimental data are taken from Ref. [30]. All the parameters are given in MeV.

| ISGMR | $\bar{\omega}$ | $20.30^{+1.69}_{-0.14}$ | 18.2 |
|-------|----------------|-------------------------|------|
|       | $\Delta$ | $4.25^{+0.69}_{-0.23}$ | 3.1 |
| ISGQR | $\bar{\omega}$ | $16.1\pm0.3$ | 14.9 |
|       | $\Delta$ | $2.4\pm0.2$ | 1.9 |

overlap with each other [17]. The smearing procedure outlined above is based on a statistical assumption: after averaging over the energy, each doorway state independently "decays" into many-quasiparticle configurations [24]. Such an assumption seems to be reasonable in view of the complexity of many-quasiparticle configurations at high excitation energies.

Per CRPA calculations of the strength functions for high-energy ("overbarrier") GRs, the doorway-state resonances overlap. In such a case, the smearing procedure lies in the replacement of $\omega$ by $\omega+iI/2$ in the CRPA equations. This replacement results in the use of the imaginary part of the single-particle potential, $\mp(i/2)I(r,\omega)$, when the radial Green's functions and continuum-state wave functions are calculated. As a result, the energy-averaged $\omega$-dependent quantities [the strength function $\bar{S}_L(\omega)$, the transition density $\bar{\rho}_L(r,\omega)$, and the direct-nucleon-escape amplitude $\bar{M}_c^L(\omega)$] can be calculated at once with the use of a radial- and energy-dependent smearing parameter in the CRPA equations. In accordance with the statistical assumption, the following parametrization for $I$ is used: $I(r,\omega)=I(\omega)f_{ws}(r,R^*,a)$, where $f_{ws}$ is the Woods-Saxon function taken with $R^*>R$ ($R$ and $a$ are the radius and diffuseness of the isoscalar part of the nuclear mean field, respectively). The calculated strength distribution and transition density of high-energy GRs are found to be almost independent of the "cutoff" radius at $R^*>(1.7-1.9)R$. The energy-dependent part of the smearing parameter $I(\omega)$ is taken in the form

$$I(\omega)=\begin{cases}\alpha\dfrac{(\omega-\Delta)^2}{1+(\omega-\Delta)^2/B^2}, & \omega>\Delta,\\ 0, & \omega<\Delta,\end{cases}\qquad(2)$$

with universal parameters. Such an energy dependence is used for the absorption potential in some versions of the optical model for nucleon-nucleus scattering [25]. The above-outlined smearing procedure has been used in Ref. [18] to describe quantitatively the gross properties of the ISGMR and ISGDR in a few nuclei. However, this procedure cannot be directly applied to evaluation of the energy-averaged escape amplitudes $\bar{M}_c^L(\omega)$ (and, therefore, the corresponding branching ratios) because of nonphysical absorption of escaped nucleons outside the nucleus. For this reason, in the present work all the energy-averaged $\omega$-dependent quantities are calculated using the "cutoff" radius $R^*=R$ together with the properly increased value of the intensity $\alpha$ in Eq. (2). Such a choice allows us to correctly describe the corresponding single-particle resonances in the energy de-
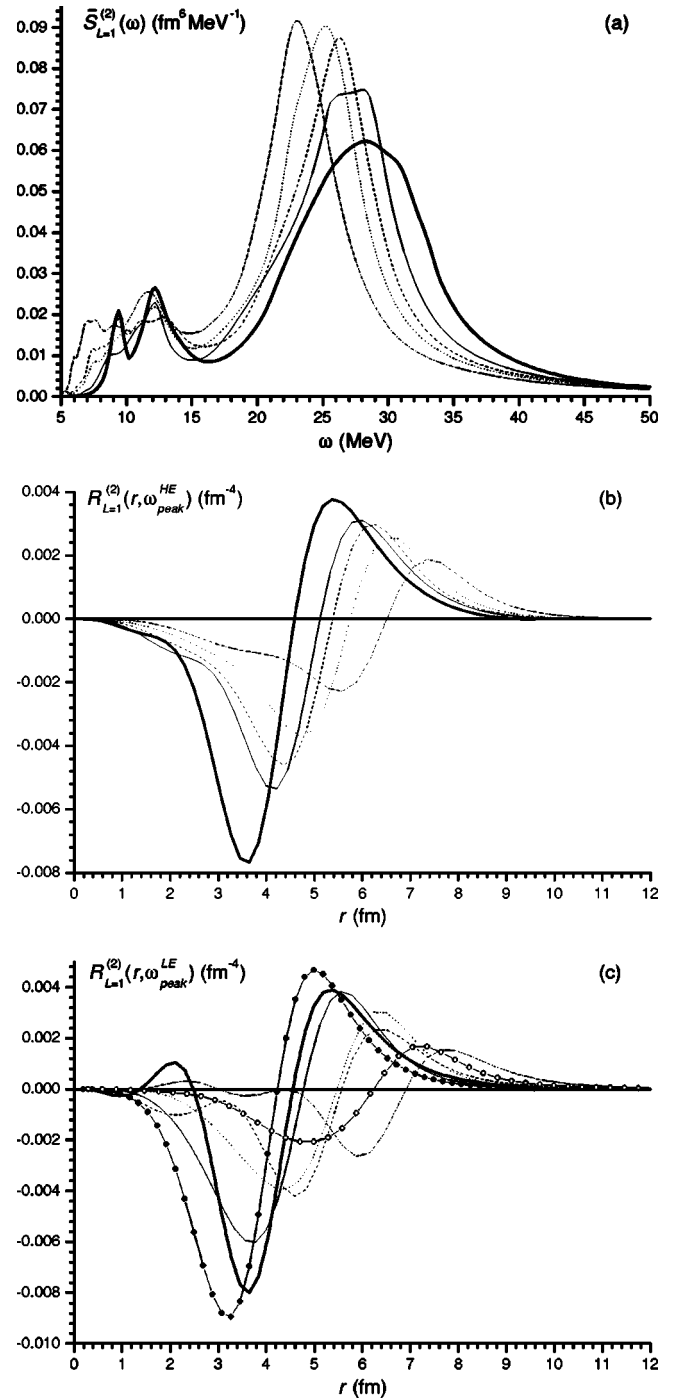


FIG. 3. (a) The energy-averaged strength function calculated for the ISGDR. (b) The reduced energy-dependent transition density calculated at the peak energy of the HE ISGDR (Table I). (c) The reduced energy-dependent transition density calculated at the peak energy of the LE ISGDR (Table I). Curves with filled circles and open circles correspond, respectively, to the additional maximum for $^{58}$Ni and $^{208}$Pb as given in Table I. Other notations on each graph are the same as in Fig. 1.

pendence of the continuum-state wave function, while the calculated gross properties of a high-energy GR are found to be almost the same within both versions of the smearing procedure. In Refs. [18,23,26] the branching ratios calculated

TABLE V. Parameters of the ISGDR calculated for different excitation-energy intervals. All the parameters are given in MeV except for $x$, which is given in percent.

| Nucleus | LE ISGDR | | | | HE ISGDR | | | |
|---|---|---|---|---|---|---|---|---|
| | $\omega_1-\omega_2$ | $\bar{\omega}$ | $\Delta$ | $x$ | $\omega_1-\omega_2$ | $\bar{\omega}$ | $\Delta$ | $x$ |
| $^{58}$Ni | 5–16 | 11.56 | 2.08 | 12 | 16–36 | 26.62 | 4.55 | 75 |
| | | | | | 16–60 | 27.94 | 6.36 | 86 |
| $^{90}$Zr | 11–18 | 13.78 | 2.10 | 10 | 18–32 | 25.42 | 3.48 | 68 |
| | 5–16 | 11.32 | 2.19 | 11 | 16–40 | 25.94 | 4.74 | 81 |
| | | | | | 16–60 | 26.69 | 6.14 | 86 |
| $^{116}$Sn | 11–18 | 13.91 | 1.99 | 11 | 18–32 | 25.09 | 3.23 | 67 |
| | 5–15 | 10.50 | 2.36 | 13 | 15–35 | 24.78 | 4.22 | 75 |
| | | | | | 15–60 | 25.91 | 6.13 | 84 |
| $^{144}$Sm | 5–15 | 10.74 | 2.22 | 12 | 15–35 | 24.20 | 4.04 | 77 |
| | | | | | 15–60 | 25.22 | 5.92 | 85 |
| $^{208}$Pb | 8–15 | 11.18 | 1.89 | 14 | 15–24 | 20.73 | 2.39 | 42 |
| | 5–15 | 9.90 | 2.55 | 17 | 15–35 | 23.02 | 3.90 | 74 |
| | | | | | 15–60 | 23.96 | 5.83 | 81 |

for a few overtones in $^{208}$Pb are overestimated because the absorption of escaped nucleons inside the nucleus is not taken into account. This shortcoming is partially eliminated in Ref. [19], where all $\omega$-dependent quantities are calculated using the smearing parameter with intermediate radius $R*=1.3R$ to take the spreading effect into account in evaluation of the branching ratios for the ISGDR in a few nuclei.

In conclusion of this subsection, we define the energy-averaged quantities suitable for description of the main properties of the isoscalar GRs. The relative energy-weighted strength function $y_L(\omega)=\omega\bar{S}_L(\omega)/(\text{EWSR})_L$ is used to show exhaustion of the respective energy-weighted sum rule (EWSR) by a particular GR. The use of the reduced energy-dependent transition density $R_L(r,\omega)=r^2\bar{\rho}_L(r,\omega)\bar{S}_L^{-1/2}(\omega)$ normalized by the condition $\int R_L(r,\omega)V_L(r)dr=1$ is convenient to compare the transition densities related to different energy regions [18]. The squared and properly normalized energy-averaged direct-nucleon-escape amplitude determines the corresponding differential partial branching ratio:

$$\frac{d\bar{b}_\mu^L(\omega)}{d\omega}=\frac{\sum_{(\lambda)}|\bar{M}_c^L(\omega)|^2}{\int_{\omega_1}^{\omega_2}\bar{S}_L(\omega)d\omega}. \tag{3}$$

These quantities show how the partial and total branching ratios are formed.

### C. Ingredients of the approach

Within the approach, a phenomenological isoscalar part of the nuclear mean field (including the spin-orbit term) and the (momentum-independent) Landau-Migdal particle-hole interaction are used as the input quantities for CRPA calculations. Parametrization of these quantities is explicitly given

in Ref. [17]. Within the RPA, the isospin symmetry of the model Hamiltonian can be restored. As a result, the isovector part of the mean field is calculated self-consistently via the Landau-Migdal isovector parameter $f'$ and the neutron-excess density (see, e.g., Ref. [23]). The mean Coulomb field is also calculated self-consistently via the proton density.

Within the CRPA, the distribution of the isoscalar dipole strength [corresponding to the probing operator with the radial part $V_{L=1}(r)=r$] can be calculated for a given model Hamiltonian. In the studies of Refs. [17,18], the Landau-Migdal isoscalar parameter $f^{ex}$ is chosen for each nucleus to make the energy of the $1^-$ spurious state close to zero. If the translation invariance of the model Hamiltonian was fully restored, the spurious state would exhaust 100% of the EWSR corresponding to the above-mentioned probing operator. Within the current version of the approach, the SS exhausts in all cases more than 92% of this sum rule, the exact percentage being dependent on the nucleus [17,18]. A small part of the spurious strength (less than 8%) is distributed mainly among isoscalar dipole $1\hbar\omega$ particle-hole-type excitations.

The calculation results presented in Sec. III are obtained with the use of model parameters taken, in the main, from previous studies of Refs. [17,18]. The mean-field parameters and the Landau-Migdal isovector parameter $f'=1.0$ are taken from Ref. [17], where the experimental nucleon separation energies have been satisfactorily described for closed-shell subsystems in nuclei with $A=90-208$. The isoscalar Landau-Migdal parameter $f^{in}$ is taken equal to 0.0875 in agreement with the systematics of Refs. [22,27], while the values of parameter $f^{ex}=-(2.7-2.9)$ are found in Ref. [18] in the manner described above for each nucleus under consideration. The universal parameters of Eq. (2) used for description of the spreading effect, $\alpha=0.125$ MeV$^{-1}$, $\Delta=3$ MeV, $B=7$ MeV, are the same as in Ref. [18], except for the $\alpha$ value ($\alpha=0.085$ MeV$^{-1}$ is used in Ref. [18], together with $R*=1.8R$).
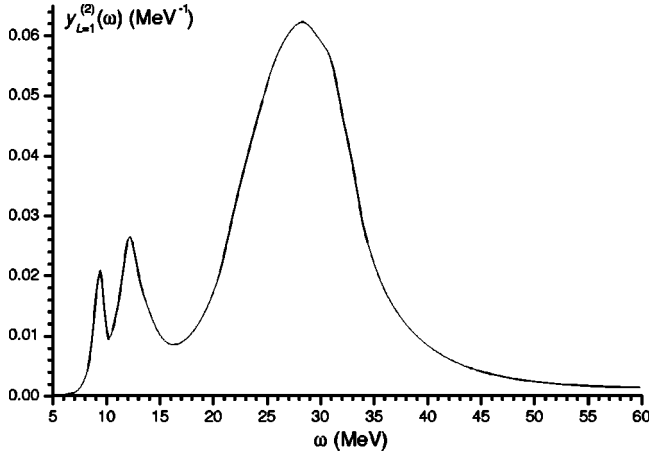
FIG. 4. The relative energy-weighted strength function calculated for the ISGDR in $^{58}$Ni.

## III. PROPERTIES OF THE ISOSCALAR GIANT MULTIPOLE RESONANCES

### A. Gross properties of the main-tone resonances

We start with a description of the main-tone resonances. This description allows us to check the quality of restoration of the translation invariance of the model within the CRPA; to check the abilities of the semimicroscopic approach because the gross properties of the isoscalar giant monopole and quadrupole resonances have been extensively studied experimentally; and to evaluate the parameters $\eta_L$ in the expression for the radial part of the second-order probing operators appropriate for microscopic studies of the overtones.

The $1^-$ spurious state associated with the center-of-mass motion is the lowest-energy main-tone state. The method to determine the properties of the SS within the CRPA is described in detail in Ref. [17] (see also Sec. II C). The method allows us to specify the value of the Landau-Migdal parameter $f^{ex}$ and to calculate the characteristics of the SS, relative isoscalar dipole strength $x_{L=1}^{SS}$, and transition density $\rho_{L=1}^{SS}(r)$. The calculated values of $f^{ex}$ and $x_{L=1}^{SS}$ for the nuclei under consideration (except for $^{58}$Ni) are given in Table I of Ref. [18]. For $^{58}$Ni we obtain $f^{ex}=-2.646$ and $x_{L=1}^{SS}=96\%$. The values $f^{ex}=-2.789$ and $x_{L=1}^{SS}=94\%$ are obtained for $^{116}$Sn taking neutron pairing into account. The radial dependence of the calculated transition density $\rho_{L=1}^{SS}(r)$ is found to be close to $d\rho(r)/dr$, where the ground-state density $\rho(r)$ is determined by the bound-state wave functions for the occupied levels:

$$\rho(r) = \sum_{\alpha=n,p} \sum_{\mu} \frac{(2j_\mu+1)}{4\pi r^2} n_\mu^\alpha [\chi_\mu^\alpha(r)]^2. \tag{4}$$

This result is quite reasonable, since the calculated relative strength $x_{L=1}^{SS}$ is close to 100%. For the same reason, the parameter $\eta_{L=1}$ in the expression for the second-order dipole operator (Sec. II A) is almost equal to the value $5\langle r^2\rangle/3$ [averaging is performed over the ground-state density of Eq. (4)]. This value is employed in many works (see, e.g., Refs. [11,13,14,17,18]). The $\eta_{L=1}$ values used in calculations of the main properties of the ISGDR in nuclei under consideration are given in Table I.

The isoscalar monopole and quadrupole GRs in the nuclei under consideration have been experimentally studied in many works [1–3,28–30]. The strength distributions deduced are presented either in terms of the peak energy $\omega_{peak}^L$ and total width $\Gamma_L$ (obtained by a Lorentzian or Gaussian fit), or in terms of the mean energy $\bar\omega_L$ and rms energy dispersion $\Delta_L$ (obtained for a certain excitation energy interval). These data are used below for comparison with the results obtained within the semimicroscopic approach. The energy-averaged strength functions $\bar S_L(\omega)$ calculated with use of the radial part $V_L(r)=r^2$ ($L=0,2$) of the first-order probing operators show prominent resonances. The corresponding peak energies and total widths are given in Table I, together with the corresponding experimental values. The relative energy-weighted

TABLE VI. Calculated partial branching ratios for direct proton decay of the HE ISGRs in $^{58}$Ni ($S_\mu=1$). The branching ratios are given in percent.

| $\mu^{-1}$ | $\bar b_\mu^{L=1}$ (15–40 MeV) | $\bar b_\mu^{L=0}$ (23–40 MeV) | $\bar b_\mu^{L=2}$ (25–40 MeV) |
|---|---|---|---|
| $(7/2)^-$ | 16.4 | 12.5 | 19.7 |
| $(1/2)^+$ | 4.7 | 6.0 | 4.1 |
| $(3/2)^+$ | 5.4 | 7.0 | 5.8 |
| $(5/2)^+$ | 6.6 | 9.7 | 7.9 |
| $(1/2)^-$ | 0.8 | 1.5 | 1.0 |
| $(3/2)^-$ | 1.1 | 2.8 | 2.1 |
| $\bar b_p^{tot}$ | 35.0 | 39.7 | 40.6 |

TABLE VII. Calculated partial branching ratios for direct nucleon decay of the HE ISGRs in $^{90}$Zr($S_\mu=1$). The branching ratios are given in percent.

| $\mu^{-1}$ | $\bar b_\mu^{L=1}$ (18–32 MeV) | $\bar b_\mu^{L=0}$ (23–39 MeV) | $\bar b_\mu^{L=2}$ (25–40 MeV) |
|---|---|---|---|
| | Neutron | | |
| $(9/2)^+$ | 10.2 | 7.6 | 14.1 |
| $(1/2)^-$ | 2.8 | 3.6 | 2.1 |
| $(5/2)^-$ | 4.6 | 5.8 | 5.0 |
| $(3/2)^-$ | 5.7 | 7.3 | 4.8 |
| $(7/2)^-$ | 4.5 | 7.2 | 7.2 |
| $(1/2)^+$ | 0.9 | 2.4 | 1.8 |
| $\bar b_n^{tot}$ | 29.6 | 40.0 | 39.9 |
| | Proton | | |
| $(1/2)^-$ | 4.0 | 4.0 | 3.0 |
| $(3/2)^-$ | 8.0 | 8.2 | 6.4 |
| $(5/2)^-$ | 5.1 | 7.3 | 6.4 |
| $(7/2)^-$ | 4.0 | 8.6 | 7.7 |
| $(1/2)^+$ 1.7 | 3.3 | 2.6 | |
| $(3/2)^+$ | 0.8 | 3.2 | 1.9 |
| $\bar b_p^{tot}$ | 24.0 | 39.5 | 31.4 |

TABLE VIII. Calculated partial branching ratios for direct nucleon decay of the HE ISGRs in $^{116}$Sn ($S_\mu=1$ and $S_\mu=v_\mu^2$ are used in the calculations of proton and neutron branching ratios, respectively). The branching ratios are given in percent.

| $\mu^{-1}$ | $S_\mu$ | $\bar{b}_\mu^{L=1}$ (15–35 MeV) | $\bar{b}_\mu^{L=0}$ (22–38 MeV) | $\bar{b}_\mu^{L=2}$ (25–37 MeV) |
|---|---|---|---|---|
| | | Neutron | | |
| $(1/2)^-$ | 0.006 | 0.04 | 0.20 | 0.06 |
| $(3/2)^-$ | 0.007 | 0.07 | 0.27 | 0.07 |
| $(7/2)^-$ | 0.011 | 0.11 | 0.16 | 0.06 |
| $(11/2)^-$ | 0.188 | 1.9 | 0.83 | 2.7 |
| $(3/2)^+$ | 0.195 | 0.84 | 0.76 | 0.45 |
| $(1/2)^+$ | 0.362 | 0.89 | 1.0 | 0.46 |
| $(7/2)^+$ | 0.862 | 4.65 | 3.7 | 4.75 |
| $(5/2)^+$ | 0.896 | 6.7 | 5.9 | 4.4 |
| $(9/2)^+$ | 0.992 | 4.9 | 5.8 | 8.7 |
| $(1/2)^-$ | 0.994 | 1.8 | 2.3 | 1.4 |
| $(3/2)^-$ | 0.996 | 3.45 | 4.8 | 3.2 |
| | $\bar{b}_n^{tot}$ | 28.8 | 25.7 | 34.7 |
| | | Proton | | |
| $(9/2)^+$ | | 4.5 | 8.2 | 9.0 |
| $(1/2)^-$ | | 2.2 | 3.6 | 1.9 |
| $(3/2)^-$ | | 3.9 | 7.3 | 4.0 |
| $(5/2)^-$ | | 1.8 | 5.3 | 2.5 |
| $(7/2)^-$ | | 1.1 | 5.6 | 3.1 |
| $(1/2)^+$ | | 0.2 | 1.8 | 1.4 |
| $(3/2)^+$ | | 0.1 | 1.3 | 0.4 |
| $(5/2)^+$ | | | 1.7 | 0.6 |
| | $\bar{b}_p^{tot}$ | 14.0 | 35.0 | 22.9 |

strength functions $y_L(\omega)=\omega\bar{S}_L(\omega)/(\text{EWSR})_L$ are shown in Fig. 1(a) ($L=0$) and in Fig. 2(a) ($L=2$) for the nuclei under consideration. Microscopically, the ISGMR and ISGQR are mainly due to $2\hbar\omega$ particle-hole-type excitations. The low-energy component of the ISGQR [Fig. 2(a)] is due to $0\hbar\omega$ excitations corresponding to single-particle transitions involving changes in both the radial and orbital quantum numbers and, consequently, having a small relative strength. The calculated strength functions are used to evaluate (for a certain energy interval) the parameters of the ISGMR and IS-GQR: mean energy $\bar{\omega}_L$, rms energy dispersion $\Delta_L$, relative strength $x_L$. These values are listed in Table II. Comparison with the available experimental data is given in Tables III and IV. The reduced transition densities $R_L(r,\omega_{peak}^L)$ calculated for the main-tone isoscalar monopole and quadrupole GRs in the nuclei under consideration are shown in Fig. 1(b) and Fig. 2(b), respectively. These transition densities are used to evaluate parameters $\eta_L$ following Eq. (1). These values are given in Table I.

**B. Properties of the ISGDR**

The gross properties of the ISGDR in nuclei under consideration are described within the approach using the iso-

scalar second-order dipole probing operator with parameters $\eta_{L=1}$ taken from Table I. The calculated energy-averaged strength function $\bar{S}_{L=1}^{(2)}(\omega)$ [Fig. 3(a)] exhibits a "bimodal" energy dependence, corresponding to the low- and high-energy components of the ISGDR (LE and HE ISGDR, respectively). As a resonance in the energy dependence of the strength function, the HE ISGDR is prominent and can be described in terms of the peak energy and total width, while

TABLE IX. Calculated partial branching ratios for direct neutron decay of the HE ISGRs in $^{144}$Sm ($S_\mu=1$). The branching ratios are given in percent.

| $\mu^{-1}$ | $\bar{b}_\mu^{L=1}$ (15–35 MeV) | $\bar{b}_\mu^{L=0}$ (21–38 MeV) | $\bar{b}_\mu^{L=2}$ (24–36 MeV) |
|---|---|---|---|
| $(1/2)^+$ | 1.9 | 2.0 | 1.0 |
| $(3/2)^+$ | 3.4 | 3.3 | 2.2 |
| $(11/2)^-$ | 5.2 | 4.9 | 9.9 |
| $(5/2)^+$ | 5.1 | 5.7 | 4.4 |
| $(7/2)^+$ | 2.6 | 4.1 | 3.7 |
| $(9/2)^+$ | 1.8 | 4.3 | 5.2 |
| $\bar{b}_n^{tot}$ | 23.1 | 35.1 | 35.3 |

the LE ISGDR is less prominent. The peak energies of both components are given in Table I together with the latest experimental data. The relative energy-weighted strength functions $y_{L=1}^{(2)}(\omega)$ are very close to those shown in Fig. 1 of Ref. [18] for the nuclei under consideration (except for $^{58}$Ni) and are not shown here. The parameters of both components calculated with the use of the above strength functions are given in Table V. Results for specific excitation-energy intervals are compared with the available experimental data deduced for the same intervals (Table III). The strength function $y_{L=1}^{(2)}(\omega)$ calculated for $^{58}$Ni is shown in Fig. 4. Because the main-tone transition density is nodeless, the energy-dependent transition density $R_{L=1}^{(2)}(r, \omega_{peak})$ calculated at the peak energy of each component exhibits one-node radial dependence [Figs. 3(b) and 3(c)].

The direct nucleon decay of giant resonances is closely related to their microscopic structure. For this reason, the decay probabilities are some of the main properties of GRs together with the energy, total width, and transition density. The use of the CRPA method together with the phenomenological treatment of the spreading effect allows us to evaluate the partial direct-nucleon-decay branching ratios for various GRs within the semimicroscopic approach. Turning to the HE ISGDR in the nuclei under consideration, we present the direct-nucleon-decay branching ratios $\bar{b}_{\mu}^{L=1}$ calculated with the use of unit spectroscopic factors $S_{\mu}$ for single-hole states in closed-shell subsystems and of unit ratio $S_{\mu}/v_{\mu}^2$ for single-quasiparticle states in open-shell subsystems (Tables VI–X). Some partial branching ratios corresponding to population of deep-hole states are not shown, but they are included in the values of the respective total branching ratios also given in the tables. The recent experimental data of Refs. [6,7] on the partial direct-proton-decay branching ratios for the HE IS-GDR in $^{208}$Pb are given in Table XI together with the corresponding calculated values obtained with the use of the experimental spectroscopic factors. Calculated for the same resonance, the differential partial proton branching ratios of Eq. (3) are shown in Fig. 5. One can see from this figure the role of the penetrability factor in formation of the HE IS-GDR in different proton-decay channels.

### C. Main properties of the ISGMR2 and ISGQR2

We describe the gross properties of the isoscalar monopole and quadrupole overtones in the nuclei under consideration, using the corresponding second-order probing operators with parameters $\eta_L$ $(L=0,2)$ taken from Table I. The overtone strength is distributed over a wide energy interval exhibiting the main peak at a high excitation energy. The $\omega_{peak}^L$ values are given in Table I. The relative energy-weighted strength functions $y_L^{(2)}(\omega)$ are shown in Figs. 6(a) $(L=0)$ and 7(a) $(L=2)$, while the parameters of the high-energy components are given in Table XII. Because the main-tone transition density has one node inside of the nucleus [$L=0$, Fig. 1(b)] or is nodeless [$L=2$, Fig. 2(b)], the overtone transition density has two nodes [$L=0$, Fig. 6(b)] or one node [$L=2$, Fig. 7(b)], respectively. The direct-nucleon-decay branching ratios $\bar{b}_{\mu}^L$, calculated for the high-energy

TABLE X. Calculated partial branching ratios for direct nucleon decay of the HE ISGRs in $^{208}$Pb ($S_{\mu}=1$). The branching ratios are given in percent.

| $\mu^{-1}$ | $\bar{b}_{\mu}^{L=1}$ (15–35 MeV) | $\bar{b}_{\mu}^{L=0}$ (25–35 MeV) | $\bar{b}_{\mu}^{L=2}$ (25–35 MeV) |
|---|---|---|---|
| | Neutron | | |
| $(1/2)^-$ | 0.7 | 0.2 | 0.2 |
| $(5/2)^-$ | 2.5 | 0.7 | 1.3 |
| $(3/2)^-$ | 1.8 | 0.6 | 0.6 |
| $(13/2)^+$ | 3.8 | 1.3 | 7.5 |
| $(7/2)^-$ | 4.3 | 1.9 | 7.2 |
| $(9/2)^-$ | 2.1 | 1.1 | 3.0 |
| $\bar{b}_n^{tot}$ | 22.4 | 24.7 | 32.5 |
| | Proton | | |
| $(1/2)^+$ | 1.2 | 2.6 | 1.2 |
| $(3/2)^+$ | 1.4 | 4.4 | 2.2 |
| $(11/2)^-$ | 0.5 | 6.2 | 2.7 |
| $(5/2)^+$ | 1.4 | 7.2 | 3.5 |
| $(7/2)^+$ 0.28 | 3.1 | 0.8 | |
| $(9/2)^+$ | 0.07 | 2.8 | 0.7 |
| $\bar{b}_p^{tot}$ | 4.9 | 31.5 | 31.0 |

components of both overtones with the use of unit spectroscopic factors, are given in Tables VI–X. Partial branching ratios for direct proton decay of the above resonances in $^{208}$Pb are also calculated with the use of experimental spectroscopic factors (Table XI).

## IV. DISCUSSION OF RESULTS AND SUMMARY

Within the CRPA-based semimicroscopic approach, all the main properties of a given GR can be described in a transparent and rather simple way using universal parameters for medium-heavy and heavy (spherical) nuclei. The symmetries of the model Hamiltonian are restored via the corresponding self-consistency conditions. In the present version of the approach the spin-orbit part of the nuclear mean field is mainly responsible for incomplete restoration of translation invariance of the model. If this part was taken equal to zero, the SS would exhaust more than 99.5% of the corresponding sum rule, while the gross properties of isoscalar GRs are essentially not changed. The self-consistency of the present version of the approach can possibly be improved, provided that the isoscalar spin-dependent part of the Landau-Migdal particle-hole interaction is taken into account. This study is outside the scope of the present work and will be addressed in a future publication.

In discussing the results, we start from the gross properties of the isoscalar GRs. Taking $^{208}$Pb as an example, one can see from the results of the semimicroscopic calculations of the relative energy-weighted strength function $y_L(\omega)$ (Fig. 8) the general tendency for changing isoscalar strength distribution with increasing excitation energy. The main components of the ISGMR2 and ISGQR2 are not very collective

TABLE XI. Partial branching ratios for direct proton decay of the HE ISGRs in $^{208}$Pb into some one-hole states of $^{207}$Tl. Experimental spectroscopic factors $S_\mu$ taken from Ref. [31] are used in calculations. Excitation-energy intervals are taken the same as in Table X. Calculation results for decays of the HE ISGDR are compared with the experimental data of Refs. [6,7]. The branching ratios are given in percent.

| $\mu^{-1}$ | $S_\mu$ | $\bar{b}_\mu^{L=1}$ | [6] | [7]$^c$ | $\bar{b}_\mu^{L=0}$ | $\bar{b}_\mu^{L=2}$ |
|---|---|---|---|---|---|---|
| $(1/2)^+$ | 0.55 | 0.65 | $2.3\pm1.1^a$ | $0.34\pm0.06$ | 1.43 | 0.66 |
| $(3/2)^+$ | 0.57 | 0.80 | | $0.61\pm0.10$ | 2.51 | 1.25 |
| $(11/2)^-$ | 0.58 | 0.29 | $1.2\pm0.7^b$ | $0.31\pm0.05$ | 3.60 | 1.57 |
| $(5/2)^+$ | 0.54 | 0.75 | | $1.07\pm0.17$ | 3.89 | 1.89 |
| $(7/2)^+$ | 0.26 | 0.02 | | | 0.81 | 0.21 |
| $\Sigma\bar{b}_\mu^L$ | | 2.51 | | | 12.24 | 5.58 |

$^a$Decay into the$(3/2)^+$ state is included.
$^b$Decay into the $(5/2)^+$ state is included.
$^c$Preliminary results.

and exhaust around one-half of the total strength (Table XII). As a result, the $A$ dependence of $\omega_{peak}^{HE}$ for these overtones is not so regular, as it takes place for more collective GRs (Table I). According to the data shown in Tables I, III, and IV the experimental energies of the ISGMR, ISGQR, and HE ISGDR in nuclei from a wide mass interval are reasonably described within the approach. The energy of the LE ISGDR in the same nuclei is described satisfactorily (Tables I and III). The energy of the recently found ISGQR2 in $^{208}$Pb, $26.9\pm0.7$ MeV [5,6], is also satisfactorily reproduced in the calculations (Table I). Thus, the calculated energies of the second isoscalar giant quadrupole and monopole resonances in the nuclei under consideration can be used as a guide to search for these GRs experimentally.

We try to elucidate the universal phenomenological description of the total width of an arbitrary GR using an appropriate smearing parameter with the saturationlike energy dependence of Eq. (2). A similar attempt applied to isovector GRs was found to be satisfactory [26]. According to this

description, the total width of low-energy GRs (except for the isobaric analogue resonance) is mainly due to the spreading effect. Such a case is realized for the main-tone isoscalar monopole and quadrupole resonances. CRPA calculations
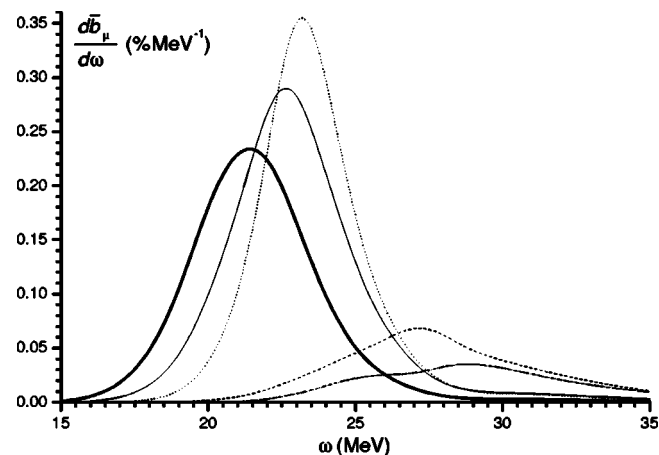




FIG. 5. The differential partial branching ratios calculated for direct proton decay of the HE ISGDR in $^{208}$Pb into several one-hole states of $^{207}$Tl ($S_\mu=1$). The thick, thin, dashed, dotted, and dash-dotted lines are for decay into $3s_{1/2}$, $2d_{3/2}$, $1h_{11/2}$, $2d_{5/2}$, and $1g_{7/2}$ states, respectively.
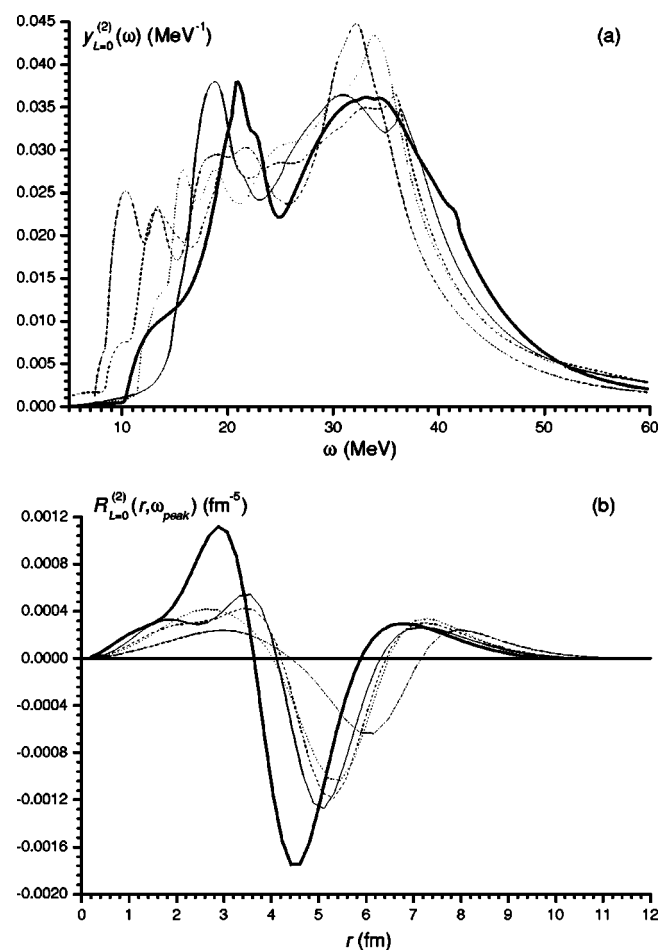
FIG. 6. (a) The relative energy-weighted strength function calculated for the ISGMR2. (b) The reduced energy-dependent transition density calculated at the peak energy of the ISGMR2 (Table I). The notations on each graph are the same as in Fig. 1.
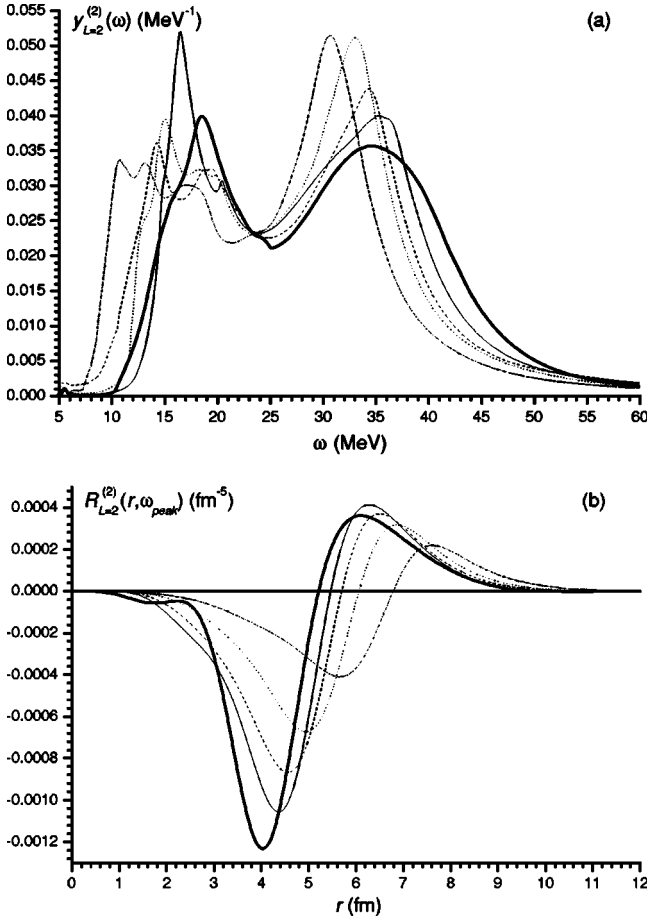
FIG. 7. (a) The relative energy-weighted strength function calculated for the ISGQR2. (b) The reduced energy-dependent transition density calculated at the peak energy of the ISGQR2 (Table I). The notations on each graph are the same as in Fig. 1.

imply that a significant part of the total width of high-energy GRs is due to the particle-hole strength distribution and the coupling to the continuum. The rest is due to the spreading effect, which also leads to the averaging of the strength distribution over the energy. We note that the widths of the ISGMR and ISGQR, and the rms energy dispersion for both components of the ISGDR are well described within our approach (Tables I and IV). The experimental total width of the ISGQR2 in $^{208}$Pb, $6.0 \pm 1.3$ MeV [5], agrees well with the rms energy dispersion calculated for the main component of
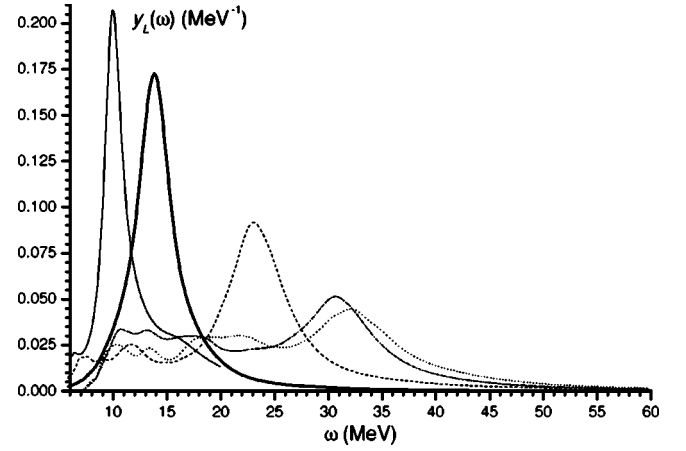


FIG. 8. The relative energy-weighted strength functions calculated for isoscalar GRs in $^{208}$Pb. The thick, thin, dashed, dotted, and dash-dotted lines are for the ISGMR, ISGQR, ISGDR, ISGMR2, and ISGQR2, respectively.

this resonance (Table XII). It is worth noting that there appears to be considerable scatter in the experimental data for the total width of the HE ISGDR [3,5,6]. This, as also the spread in the experimental relative strengths $x_L$, is apparently attributable to the uncertainties in the subtraction of the underlying continuum in the analysis of the $(\alpha, \alpha')$-reaction cross sections. For this reason we do not compare in the present work the calculated $x_L$ values (Tables II and V) with the corresponding experimental data. Nevertheless, one can compare the calculated (Fig. 4) and experimental (Ref. [4]) strength functions $y_{L=1}^{(2)}(\omega)$ for $^{58}$Ni and find satisfactory agreement.

As expected, the radial dependence of the one-node transition density $R_L(r, \omega_{peak})$ for the ISGMR and HE ISGDR [Figs. 1(b) and 3(b)] is rather close to that of the corresponding transition density calculated within the scaling model [32], provided the ground-state density of Eq. (4) is used in the calculations. This can be seen, for instance, in Fig. 2 of Ref. [18]. We note also that the difference in the transition densities calculated at the peak energy of each ISGDR component is not large enough [Figs. 3(b) and 3(c)] to warrant exotic alternative explanations for the nature of the LE ISGDR. As is also expected, the overtone transition density has one extra node inside the nucleus relative to the main-tone transition density [Figs. 1(b), 2(b), 3(b), 6(b), and 7(b)]. We

TABLE XII. Parameters of the ISGMR2 and ISGQR2 calculated for a certain excitation-energy interval. All the parameters are given in MeV except for $x$, which is given in percent.

| | ISGMR2 | | | | ISGQR2 | | | |
|---|---|---|---|---|---|---|---|---|
| Nucleus | $\omega_1 - \omega_2$ | $\bar{\omega}$ | $\Delta$ | $x$ | $\omega_1 - \omega_2$ | $\bar{\omega}$ | $\Delta$ | $x$ |
| $^{58}$Ni | 23–40 | 31.1 | 4.7 | 52 | 25–40 | 32.5 | 4.1 | 45 |
| $^{90}$Zr | 23–39 | 30.6 | 4.4 | 51 | 25–40 | 32.2 | 4.1 | 48 |
| $^{116}$Sn | 22–38 | 29.6 | 4.6 | 50 | 25–37 | 31.3 | 3.3 | 40 |
| $^{114}$Sm | 21–38 | 29.2 | 4.7 | 56 | 24–36 | 30.4 | 3.3 | 43 |
| $^{208}$Pb | 25–35 | 30.2 | 2.8 | 34 | 25–35 | 30.0 | 2.6 | 38 |

further note that the use of the modified smearing procedure (as compared with that of Ref. [18]) leads to practically the same results, as can be seen from a comparison of the data of Tables II and V with those of Tables I and II of Ref. [18].

The use of the modified smearing procedure (Sec. II B) allows us to describe within the present approach the direct-nucleon-decay branching ratios for high-energy GRs. The corresponding calculation results obtained for the isoscalar overtones in the nuclei under consideration are given in Tables VI–X. For the ISGDR, the total direct-nucleon-decay branching ratio decreases with decrease of the peak energy (with increase of the mass number). The relative change is larger for the total proton branching ratios due to the difference in the penetrability factors. We note that the results of Ref. [19], where the main shortcoming in evaluation of the direct-nucleon-decay branching ratios for high-energy GRs was eliminated (Sec. II B), are close to those of Tables VI–XI.

The recent experimental data of Refs. [6,7] on partial direct-proton-decay branching ratios for the HE ISGDR in $^{208}$Pb are satisfactorily described within the present approach, provided that experimental spectroscopic factors for the final single-hole states of $^{207}$Tl (Table XI) are taken into account. In Ref. [6] direct neutron decay of the same resonance into the final states of $^{207}$Pb from the excitation-energy interval 0–6 MeV has also been observed. The deduced branching ratio $23\pm5$ % reasonably agrees with the value 15.2% obtained with the use of a unit spectroscopic factor for the corresponding one-hole states (Table X). A reasonable description of the above data allows us to infer that the calculation results shown in Tables VI–IX will be useful for the analysis of forthcoming experimental data on direct nucleon decays of the HE ISGDR in several medium-heavy and

heavy nuclei [8]. Some evidence for direct proton decay of the ISGQR2 in $^{208}$Pb in coincidence $(\alpha, \alpha' p)$ experiments has been found recently [5,6]. It allows us to hope that the calculated parameters of the ISGQR2 and ISGMR2 (including the energy, total width, transition density, and branching ratios for direct nucleon decay) would also be useful in experimental searches for these resonances.

In conclusion, we extend a CRPA-based partially self-consistent semimicroscopic approach to describe direct nucleon decay of high-energy giant resonances. The main properties of the isoscalar overtones (ISGDR, ISGMR2, ISGQR2) in a few singly- and doubly-closed-shell nuclei are described within the approach and found to be in reasonable agreement with available experimental data, including the latest ones. The ability of the approach to describe the maintone resonances is successfully checked. Predictions concerning forthcoming experimental data for the isoscalar overtones are also presented.

[1] M. N. Harakeh and A. van der Woude, *Giant Resonances: Fundamental High-Frequency Modes of Nuclear Excitations* (Oxford University Press, New York, 2001).

[2] H. L. Clark, Y.-W. Lui, and D. H. Youngblood, Phys. Rev. C **63**, 031301(R) (2001).

[3] M. Itoh *et al.*, Phys. Lett. B **549**, 58 (2002); M. Uchida *et al.*, Phys. Rev. C (in press).

[4] B. K. Nayak *et al.*, contribution to the COMEX1 Conference, La Sorbonne, France, 2003, Book of Abstracts, p. 112.

[5] M. Hunyadi *et al.*, Phys. Lett. B **576**, 253 (2003).

[6] M. Hunyadi *et al.*, Nucl. Phys. A (in press).

[7] U. Garg, Nucl. Phys. A (in press); (private communication).

[8] M. Fujiwara, U. Garg, and M. N. Harakeh (private communication).

[9] A. Erell *et al.*, Phys. Rev. C **34**, 1822 (1986); R. G. T. Zegers *et al.*, *ibid.* **63**, 034613 (2001); D. L. Prout *et al.*, *ibid.* **63**, 014603 (2001).

[10] R. G. T. Zegers *et al.*, Phys. Rev. Lett. **90**, 202501 (2003).

[11] N. Van Giai and H. Sagawa, Nucl. Phys. **A371**, 1 (1981).

[12] S. E. Muraviev and M. G. Urin, Bull. Acad. Sci. USSR, Phys. Ser. (Engl. Transl.) **52**, 123 (1988).

[13] G. Colò *et al.*, Phys. Lett. B **485**, 362 (2000).

[14] S. Shlomo and A. I. Sanzhur, Phys. Rev. C **65**, 044310 (2002).

[15] D. Vretenar, A. Wandelt, and P. Ring, Phys. Lett. B **487**, 334 (2000).

[16] A. Kolomietz, O. Pochivalov, and S. Shlomo, Phys. Rev. C **61**, 034312 (2000).

[17] M. L. Gorelik, S. Shlomo, and M. H. Urin, Phys. Rev. C **62**, 044301 (2001).

[18] M. L. Gorelik and M. H. Urin, Phys. Rev. C **64**, 047301 (2001).

[19] M. L. Gorelik and M. H. Urin, nucl-th/0209094 v1; M. L. Gorelik, I. V. Safonov, and M. H. Urin, Proceedings of the X International Seminar on Electromagnetic Interactions of Nuclei at Low and Medium Energies, INR of RAS, Moscow, 2004, p. 50; M. L. Gorelik and M. G. Urin, Phys. At. Nucl. **66**, 1883 (2003).

[20] S. E. Muraviev *et al.*, Phys. Rev. C **59**, 2040 (1999).

[21] S. Shlomo, V. M. Kolomietz, and B. K. Agraval, Phys. Rev. C **68**, 064301 (2003).

[22] A. B. Migdal, *Theory of Finite Fermi Systems and Properties of Atomic Nuclei* (Nauka, Moscow 1983) (in Russian).

[23] M. L. Gorelik and M. H. Urin, Phys. Rev. C **63**, 064312 (2001).

[24] S. E. Muraviev and M. H. Urin, Nucl. Phys. **A572**, 267 (1994).

[25] C. Mahaux and R. Sartor, Nucl. Phys. **A503**, 525 (1989).

[26] V. A. Rodin and M. H. Urin, Nucl. Phys. **A687**, 276c (2001).

[27] J. Speth, E. Werner, and W. Wild, Phys. Rev. C **33**, 127 (1977).

[28] D. H. Youngblood *et al.*, Phys. Rev. C **23**, 1997 (1981).

[29] D. H. Youngblood, H. L. Clark, and Y.-W. Lui, Phys. Rev. Lett. **82**, 691 (1999).

[30] Y.-W. Lui, H. L. Clark, and D. H. Youngblood, Phys. Rev. C **61**, 067307 (2000).

[31] I. Bobeldijk *et al.*, Phys. Rev. Lett. **73**, 2684 (1994).

[32] S. Stringari, Phys. Lett. **108B**, 232 (1982).